



**Computational Studies of Ni(II) photosensitizers
complexes containing 1, 1'-
bis(diphenylphosphino)ferrocene and dithio ligands.**

Journal:	<i>Canadian Journal of Chemistry</i>
Manuscript ID	cjc-2019-0168.R2
Manuscript Type:	Article
Date Submitted by the Author:	08-Feb-2020
Complete List of Authors:	BRAHIM, Sefia ; University Dr Tahar Moulay of Saida, Chemistry department BRAHIM, Houari; University Dr Tahar Moulay of Saida, Chemistry department HUMBEL, Stéphane; Aix-Marseille Université RAHMOUNI, Ali; Université Dr Tahar Moulay de Saida, Chimie
Is the invited manuscript for consideration in a Special Issue?:	Not applicable (regular submission)
Keyword:	Ni complexes, TD-DFT calculations, Photosensitizer, Electronic spectra

SCHOLARONE™
Manuscripts

Computational Studies of Ni(II) photosensitizers complexes containing 1, 1'-bis(diphenylphosphino)ferrocene and dithio ligands.

Sefia BRAHIM^a, Houari BRAHIM^c, Stéphane HUMBEL^b, Ali RAHMOUNI^{a*}

^a Modeling and Calculation Methods Laboratory, University of Saida, B.P. 138, 20002 Saida, Algeria

^b Aix Marseille Université, Centrale Marseille, CNRS, iSm2 UMR 7313, 13397, Marseille, France.

^c Department of Chemistry, University of Saida, Saida, 20000, Algeria

*Corresponding author

rahmouniali@hotmail.com

Abstract

Detailed theoretical studies of Ni(II) complexes in a distorted square planar form and containing dithio and (P,P) chelating ligands were performed. These Ni(II) complexes are investigated for their use in dye-sensitized solar cells (DSSC). Structures and UV-Vis spectra are calculated at density functional theory (DFT) and time-dependent density functional theory (TD-DFT) theories using B3LYP and CAM-B3LYP functionals and 6-31G(d,p) and 6-31G+(d) basis set. Geometry optimizations result in excellent agreement with the experimental results. Moreover, the analysis of the frontier molecular orbitals (FMOs) allowed a detailed assignment and a clear analysis of the electronic transitions. The TD-DFT calculations reproduce the main spectroscopic properties observed and substituent effects. The results reveal that all absorption spectra are characterized by mixed character mainly dominated by metal to ligand and ligand to ligand charge transfer (MLCT and LLCT). We unveil how the substituent variations affect the DSSCs features of the complexes.

Keywords

Ferrocene, Ni complexes, TD-DFT calculations, Photosensitizer, Electronic spectra

Introduction

The improvement of dye-sensitized solar cells (DSSCs) still attracts considerable research.¹⁻³ To obtain more efficient DSSCs, the improvement of the photoanode, via the development of the sensitizing dye, is one promising approach⁴. Several theoretical and experimental investigations have been performed to find sensitizers with good performance and low manufacturing cost.^{5,6} The ideal dye must (i) absorb UV and visible light, extending into the near-IR region with high extinction coefficients, (ii) should exhibit strong adsorption on the surface of semiconductor TiO₂, and (iii) for the charge-separation lifetime, its unoccupied orbitals (particularly the LUMO) must be higher in energy than the conduction band of the semiconductor while its HOMO energy must be lower than the redox potential of the electrolyte.^{1,2,7} Numerous dye sensitizers, using a wide range of transition metal complexes, have been proposed and synthesized in recent years.⁸⁻²⁹ Among DSSCs on TiO₂ semiconductor, the cells containing Ru(II) based sensitizers are the most efficient.^{15,16,30} However, as suggested by Linfoot et al. their use could present serious drawbacks, due to the low metal availability and its toxicity.¹² Hence, some other research groups have synthesized and examined other complexes using more abundant and inert metals such as platinum.^{20,22} An important step forward is to increase the light absorption properties of Pt complexes. To do so, Singh et al. and Du et al. have prepared a family of square planar Pt(II) (diimine)/diphosphine-(dithiolate) complexes containing 1,1- dithioligands [dithiocarbimate²⁻, 1-ethoxycarbonyl-1-cyanoethylene-2,2-dithiolate (**ecda**²⁻). They indicate that these complexes have good photophysical and electrochemical properties.^{20,22}

Linfoot et al. present the first complex of nickel (II) showing DSSC functions.¹² Because it contains diimine and dithiolate ligands, the complex exhibits satisfactory light harvesting properties, convenient redox potential, and sufficient charge-separation lifetime. From DFT and TD-DFT calculations using B3PW91 functional results compared to experimental data, the authors conclude that Ligand-Ligand Charge Transfert (LLCT) transitions occur in the complex and allow the appropriate electron injection to the TiO₂ semiconductor. The authors also attribute the low photocurrents to short-lived excited states of the complex.¹² To take advantage of square planar shape of the first coordination shell, which has a strong crystal field, Kumar et al. synthesized, characterized and investigated the spectroscopic and electrochemical properties of four nickel(II)diimine dithiolato complexes

with the same first coordination shell of Linfoot's complex.²⁵ From DFT calculations as well as experimental investigations, Kumar et al. showed that the four complexes exhibit an absorption band due to LLCT transition from the HOMO (mainly located on the dithiolate), to the LUMO (located on the diamine). It was also noted that the oxidation of the four complexes takes the positive charge away from the TiO₂ semiconductor, so these complexes can be considered as efficient light harvesting.²⁵ Homoleptic complexes of nickel with 1, 2 dithiolene also exhibit DSSCs functions.³¹ Because they contain only sulfur atoms in the first coordination shell, these complexes absorb near IR radiation and can easily inject their electrons into the conduction band of the semiconductor.³¹ Metal complexes with 1,3-dithiole-2-thione-4,5-dithiolate (dmit) ligands are an important class of functional materials. Therefore DFT and TD-DFT using B3LYP and CAM-B3LYP exchange correlation functional with CEP-121G effective core potentials and 6-31++G basis sets calculations were carried out to examine the performance of the model [(CH₃)₂][Ni(dmit)₂] complex as a sensitizer. Special attention was paid to its spectroscopic and adsorption on TiO₂ surface properties.³² The complex exhibits physisorption on TiO₂ surface due to dispersion forces between its dmit π system and the atoms of this surface. However, this adsorption mode is unfavorable for electron injection on TiO₂ conduction band. Furthermore TD-DFT results show that the model complex doesn't absorb significantly in the visible spectrum region. Finally, the authors conclude that these dmit complexes are unsuitable sensitizer for DSSC.

It's well known that ferrocenes exhibit good optical properties. Several studies in literature proposed heteropolymetallic complexes containing ferrocene to DSSC application.^{21,26,33-36} UV and visible light conversions by Ni, Pd, and Pt complexes incorporated 1,1- dithioligands and ferrocene derivatives have been explored and it was shown that the Ni(II) complexes were the best candidate for solar cells sensitizer.³⁶ 1,1'-bis(diphenylphosphino) ferrocene (dppf) contains P donors with ability to link to a variety metal atoms to generate heteronuclear complexes exhibiting effective photophysical and electrochemical properties which make them the subject of several recent scientific investigations to develop new dye sensitizers.^{23,37-39}

This paper is concerned with theoretical investigations of Ni complexes : Ni(dppf)(p-tolylsulfonyl dithiocarbamate) **1**, Ni(dppf)(p-chlorobenzene sulfonyl dithiocarbamate) **2**, Ni(dppf)(p-bromobenzene sulfonyl dithiocarbamate) **3**, and: Ni(dppf)(1-ethoxycarbonyl-1-cyanoethylene-2,2-dithiolate) **4**. 2D structures of these complexes are shown by figure 1. K. Singh et al. reported that these complexes show high light conversion efficiencies.²³

Additionally to the (P, P) chelating ligand (dppf), these complexes also involve different (S, S) coordinating ligands which are aromatic sulfonyl dithiocarbamate (*dte*²⁻) and dithiolate derivatives (*ecda*²⁻). It's worth noting that these ligands present considerably delocalized π -orbitals which interact with d and p metal orbitals to stabilize square planar geometry of the complexes and enhance the charge transfer. DSSC functions of the four complexes were experimentally investigated. The authors conclude that this complexes feature high light conversion efficiencies.

As mentioned before, combination of experimental and DFT and TD-DFT based theoretical investigations of sensitizers help to clearly identify its molecular properties that influence its light conversion efficiency. Theoretical studies of the complexes **1**, **2**, **3**, and **4** may complete and provide clear explanations of the published experimental investigations results. Particular attention is paid to the relationship between (S, S) ligand features and structural and electrochemical properties and UV-Visible spectra of the complexes **1**, **2**, **3**, and **4**. To this end, quantum calculations at density functional theory level were carried out. The obtained frontier orbitals of the complexes are analyzed and compared. Theoretical spectra of the four complexes are established in solvent at vertical electron transition and without spin-orbit effect.

Computational details

The ground state geometry S_0 of the **1-4** Ni(II) complexes was optimized using the popular hybrid functional B3LYP (the combination of Becke's 3-parameter hybrid treatment with the Lee–Yang–Parr correlation functional).⁴⁰ Cl and Br atoms were described using the 6-31+G (d) Pople basis set, and the remaining atoms were described using 6-31G(d,p) ones.⁴¹ The geometric structure of complexes **1-3** taken from X-ray data was the starting point of a full optimization in gas-phase and in CH₂Cl₂ solvent.²³ The X-ray data of the complex **4** are not available; however these data are available for its Pd analog. The Pd atom was replaced by Ni in the experimental geometry of the Pd complex to build the starting point of the geometry optimization of complex **4**. All optimized structures were characterized as minimum on potential surface by frequencies calculations. It to be noted calculations at different level of theory have been carried out. However, only the results obtained at the above cited level are analyzed in results and discussions section.

In order to study the electronic spectroscopy properties of these complexes, the TD-DFT scheme was applied.⁴² This is indeed an effective tool to investigate the interactions and

transitions between ground and excited states of organometallic complexes. This level of theory can be as accurate as correlated ab initio techniques for the description of excited states.⁴³⁻⁴⁷ As it will be detailed below, the frontier molecular orbitals analysis show that metal to ligand and ligand to ligand long-range charge transfers can held in the transitions from ground state to the first excited state of the studied complexes. This was confirmed by the small values obtained in the lambda diagnostic calculations (smaller than 0.30).⁴⁸ Then TD-DFT calculations were carried out using 6-31+G(d) basis set and CAM-B3LYP hybrid exchange correlation functional including long range corrections.⁴⁹ This functional provided appropriate results in the investigations of nickel complexes.^{10,32} The geometries optimized at CAM-B3LYP/6-31+G(d) level, were used in the calculations of vertical excitation energies. The experimental spectra of Ni(II) complexes are determined in CH₂Cl₂ solution. So, the dichloromethane solvent effects were included by the mean of polarizable continuum model (PCM) in DFT and TD-DFT calculations.⁵⁰ All the calculations have been performed with Gaussian09 and Gabedit program packages.^{51,52}

Results and discussions

Ground state structural aspects

The structures of complexes **1-4**, as optimized at B3LYP/6-31G(d,p) level and their atomic numbering are shown in Figure 2.

Table 1 shows the parameters of the optimized geometries of the first coordination shell of nickel obtained in gas-phase and the corresponding experimental data published by K. Singh et al.²³

The optimized geometric parameters in the gas phase and in CH₂Cl₂ of complexes **1-3** are in good agreement with the experimental data. The computed bond lengths and bond angles have slightly higher or lower values than in the crystal structure. These feeble differences can be attributed, at least in part, to the environment: theoretical calculations refer to the isolated molecules, while the experimental values appertain to the molecules in the crystal. Because complex **4** did not diffract successfully, only X-ray data of complexes **1**, **2**, and **3** were provided by K. Singh et al.²³ Confident in the level of computation, we performed the geometry optimization of the ground state of the complex **4** at the same level.

The calculated bond lengths Ni-P and Ni-S are in the range of 2.203-2.259 Å in dichloromethane and 2.187-2.239 Å in gas-phase; which are close to the experimental values

2.201(1)-2.223(1)Å. Similar agreement was noted by Paes et al. in theoretical studies of Ni complexes containing only sulfur atoms in its first coordination shell.³² The computed bond angles around nickel atom also in very good agreement with X-ray values. As noted by Pastorek et al in their experimental studies of dithiocarbamate complexes of nickel(II) with 1-1'-bis(diphenylphosphino)ferrocene the first Ni coordination shell has a distorted square planar geometry.⁵³ It shall be noted that in all the complexes the P(1)-Ni-P(2) bond angles are greater than 90° by about 10° (100°-102°), and the S(11)-Ni-S(13) bond angles are smaller than 90° by about 10° (77° - 80°). These two deviations are also obtained in a model computation (Figure 3), and we attributed the deviations to a kind of size effect of the carbon atom in the 4-membered ring (Ni-S-C-S). Because the carbon atom is a small atom, the S(11)-Ni-S(13) angle is smaller than normal. This leaves room for the phosphine substituents around the planar nickel atom. The dihedral angles Ni-S-C-S are in the range of 5 to 9° in all studied complexes. Hence, this four-membered ring is essentially planar, which favors π conjugation with the imine moieties. C-N bond distances confirm the conjugation. Their lengths are in the range of 1,285-1,376Å (B3LYP results) and 1.286-1.302 Å (experimental X-rays'). These values are larger than typical C=N double bonds (1.27 Å), yet smaller than usual single bonds (1.40Å). The conjugation effect can be seen also on X-rays' C-S bond distances: at about 1.73Å, they are shorter than typical single C-S bond lengths (1.81Å). This indicates the fractional double character of this bond in these complexes.^{20,53-55} S-N bond distances are in the range of 1.678-1.692 Å (B3LYP), close to a single bond.⁵⁶ In complexes **1**, **2** and **3**, the phenyl ring of the sulfonic group is perpendicular to the four membered ring S(11)-M-S(13)-C(12). This geometry unfavors π electrons delocalization beyond the imine, In the complex **4** the C(12)-C(14), C(14)-C(15) and C(15)-N(16) bond distances are calculated at 1,376, 1.474 and 1.165 Å respectively using (B3LYP). The first C-C bond has a distance very close to C-C double C-C bond (1.34 Å), when the second has an intermediate distance between double and single C-C bond (1.54 Å). The C-N bond has a typical C-N triple bond distances. It should be concluded a π electrons delocalization on Ni-S-C-S and cyanoethene (cye) moieties.

Frontier molecular orbitals

The analysis of the frontier molecular orbitals (FMOs) is very helpful to study electronic and electrochemical properties of the complexes, on which depend their DSSC functions.^{6,10,24,32} This analysis allows the identification of the electronic transitions related to the appearance of bands in the electronic absorption spectra. The plot of computed frontier

molecular orbitals of **1-4** complexes with B3LYP are shown in Figure 4 and the HOMO-LUMO diagram shown in Figure 5 summarizes the results together with (i) experimental energy levels of the TiO₂ semiconductor conduction band (-4.00 eV)⁵⁷ and (ii) the experimental redox potential of I^-/I_3^- (-4.80 eV).⁵⁸ A graphical representation of the composition of the five highest occupied and five lowest unoccupied molecular orbitals are showed in Figures 6 and 7 respectively.

The HOMO of complexes **1-4** are at about the same energy level. These remarks are consistent with their shape, which indicates that similar interactions occur between Ni orbitals and those of the atoms of the first coordination shell. These results are in agreement with the anodic redox potential, which indicates that the HOMOs are lower than the I^-/I_3^- redox potential, and that the variation of the substituent of the thioligand has no effect on the HOMOs.²³ This means that these dyes would ensure efficient dye regeneration.^{1,2,7} LUMO of complexes **4** is about 0.4 eV lower than LUMO of complexes **1-3**, which have similar energy values. These complexes exhibit calculated virtual orbitals energies higher than the conduction band edge of TiO₂, which would be a sufficient driving force for electron injection.^{1,2,7} The complexes **1-3** exhibit similar HOMO-LUMO gap while complex **4** shows a smaller one and that indicates that it might very well be less stable than the former ones. The HOMO-LUMO gap is related to intramolecular charge transfer. It is a parameter of electronic transport properties and stability of molecules.^{59,60} The molecules having a large energy gap, need large energy to excitation and exhibit good stability.^{60,61} The molecules having a small energy gap are more polarizable with low stability, they need small energy to excitation.^{53,61}

The values of HOMO–LUMO gap for the studied complexes present the most important information about the electronic absorptions; these values specify the energy transition of an electron from the HOMO to the LUMO which can be used to predict the performance of the solar cell. The HOMO-LUMO gaps are ranked in ascending order $\Delta E_4 < \Delta E_2 < \Delta E_3 < \Delta E_1$. Similar ranking is obtained from the experimental peak potential separation derived from cyclic voltammogram.²³ The results show that the solvent effect pushes down the HOMO and LUMO energy level and increases slightly the HOMO–LUMO energy gap. Upon changing the substituent element X, we note a small effect on the HOMO and LUMO levels. Due to distorted square planar geometry of first coordination shell, d-orbitals of Ni (II) interact differently with ligand orbitals; t_{2g} type d_{yz} , d_{xz} and d_{z^2} contribute to the more stable orbitals HOMO, HOMO-3 and HOMO-4 when e_g type orbitals d_{xy} and $d_{x^2-y^2}$ contribute to the virtual orbitals.

The HOMO of complexes **1-3** consists of d_{yz} orbital of the Ni atom and p orbital of the S atoms of dithiocarbamate (dtc) where, in complex **4**, there is a contribution of π_{CN} and π_{CC} bonding type orbitals of cyanoethylene (cye) to this orbital. $ecda^{2-}$ and aromatic sulfonyl dithiocarbamate²⁻ (dtc^{2-}) provide electron delocalization beyond NiS₂ bond. The substitution of dtc^{2-} by $ecda^{2-}$ induces a large HOMO delocalization. HOMO of the four complexes are based on Ni atomic orbital which indicate that their regeneration occur by electronic transfer from electrolyte to the nickel atom. The electronic transition from HOMO orbital should be of MLCT character as required for dye sensitizer.⁶ HOMO-1 in complex **4** results from interactions between d_{xz} of Ni, p of S, and π_{CN} and π_{CC} of cye orbitals. In **4**, it has an energy closer to HOMO than in the 3 other complexes.

Both HOMO-1 and HOMO-2 are a mixture of $\pi_{cp-Ferro}$ orbital of cp-ferro fragment and d_{xz} (HOMO-1), $d_{x^2-y^2}$ (HOMO-2) orbital of Fe in **1-3**, so they are essentially ferrocene fragment orbitals. The same remarks are noted for HOMO-2 and HOMO-3 of complex **4**. The HOMO-3 of complexes **1-3** is almost a pure d_{xz} orbital of Ni. We note small contributions of p orbital of N and S atoms of SCS. The HOMO-4 of **1-4** is mainly the d_{z^2} of Ni atom with small contribution of pS (SCS). The orbital p_x and p_y of Cl and Br atoms in complex **2, 3** contribute in different orbitals that have a low energy as p_xCl in HOMO-11 and p_xBr in HOMO-8. It is worth noting also that phosphorus atoms have a small contribution of p orbital in low energy levels.

In all complexes the LUMO is a mixture of d_{xy} and $d_{x^2-y^2}$ of Ni atom and anti-bonding π^* orbital of SCS. We note a small contribution of π_{PC}^* and π_{CC}^* of phenyl moiety ($pph2-1, pph2-2$). The LUMO+1 of 1-3 complexes is mixture of π_{SCS}^* and π_{CC}^* orbital of ph, noting the slight contribution of π_{CN}^* and π_{SN}^* of dtc^{2-} . Likewise the contribution of π_{CC}^* orbital of $pph2-1, pph2-2$. On the other hand, the LUMO+1 in **4** is a combination of π_{CN}^* of cye, π_{CC}^* orbital of $pph2-1$ and $\pi_{SCS}^*, \pi_{CO_2}^*$ orbitals. The LUMO+2, LUMO+3 and LUMO+4 for all complexes are essentially composed from π_{PC}^*, π_{CC}^* orbital of $pph2-1$ and/or $pph2-2$ and π_{CC}^* orbital of ph. It can also be noted that the ferrocene moiety has a modest contribution of dFe and $\pi_{cp-ferro}^*$ in LUMO+7, LUMO+8 and LUMO+9. It is noted that the supposed anchoring CO₂ fragment orbitals contribute only in the LUMO+1. Hence, it is the photo excitation to this orbital that allows the electron injection to the TiO₂ semiconductor conduction band.^{1,2,7}

UV-visible absorption spectra

In this section, we study the absorption spectra of complexes **1-4**. The original experimental absorption spectra of complexes **1-4** published by K. Singh et al. have been regrouped on one graph so they can be compared one to the other (Figure 8).²³ All complexes display a similar somewhat broad absorption band in visible region (250-350 nm). These bands were attributed to the intraligand charge-transfer (ILCT) transitions in the first coordination shell of nickel atom.²³ Three bands were observed in this region for the complexes **1** and **4** while only two bands were observed for complexes **2** and **3**. The not observed band at 267 nm for complexes **2** and **3** can be interpreted as an effect of the substitution of methyl group by Cl or Br atom on its absorbance. It is to be noted that the structurally ligand different complexes **1** and **4** have similar ILCT transitions. Moreover, the studied complexes show a medium broad absorption bands in the ultra violet region (421-475 nm).

K. Singh et al. as some research groups have assigned these low energy bands to the d-d transitions from the d_z^2 orbital of Fe and to the LMCT transition from dithio ligand to nickel ion.^{23,36,62} The complexes **2**, **3** and **4** display only one absorption band in the range from 480 nm to 400nm when complexes **1** show two bands in this spectral region. For complexes **2** and **3**, the absence of the absorption band at 421 nm is to be related to the substitution of the methyl group by Cl or Br atom. Complexes **2** and **3** have very similar electronic spectra, which indicate that the substitution of the Cl by a Br has little effect. The absorption band at 328 nm is observed only in the complex **4** spectrum. The changes induced on π orbitals features by the substitution of cye by ecd²⁻ are reflected by the differences on the absorptions of complexes **1** and **4** in UV region. The experimental absorption spectra of complexes **1-4** were used as a guide for the analysis of the computed absorption spectra. TD-DFT results discussed below will help to interpret the differences between the four spectra.

The wavelength, oscillator strengths of the 50 first singlet calculated transitions for complexes **1**, **2**, **3** and **4** have been converted to simulated spectra via Gaussian convolution using full-width at half-maximum(FWHM) of 4nm. The figures 9, 10, 11 and 12 show the simulated and experimental spectra of complexes **1**, **2**, **3**, **4** respectively.

It should be noted that the inclusion of the solvent dielectric field, as considered in the PCM solvation model, improves the agreement between simulated and experimental absorption spectra of complex **1**. When non-specific solvent effects are considered a systematic slight hypsochromic shift (blue shift) is observed on most of the bands.⁶³ Red shifts are noted on reduced number of bands particularly in the low energy region.

For all the complexes (**1**, **2**, **3**, and **4**) simulated and experimental spectra are in significant agreement. The observed bands are well reproduced both in transition energy and relative intensity. Both in simulated and experimental, high energy absorptions are largely more intense than those of low energy.

TD-DFT calculations indicate that the four complexes absorb upper 520 nm at the same five wave lengths with the same intensities, which is interpreted by the negligible effect when the substituent R is modified. It is noted for the four complexes that these transitions are not pure HOMO to LUMO electron transfer. Furthermore, the atomic orbital d of Ni contribute less than 50% to these orbitals which allow us to describe these transitions as mixed d-d, metal to ligand, and ligand to ligand charge transfer (d-d, LLCT, MLCT) character. Experimentally, Singh et al suggested that the absorptions in this spectral region are due to Ni d-d transition.²³ Singh et al, ascribed the observed band at 560 nm in solid as Nujol mull of Ni complex with the same first coordination shell of the studied complexes to d-d transition.²⁰

In the range from 530 to 345 nm of simulated spectra the four complexes exhibit five bands having slightly the same wave length and oscillator strength. Only two bands are observed for complex **1** and **4** when one band is observed for complex **2** and **3**. These transitions of mixed MLCT and LLCT character are local and occur on ddppf moiety. The calculated transitions about 467 nm can be considered equivalent to the observed ones at 478 and 465 nm for the complexes **1** and **4** respectively. The calculated bands about 465 nm for complexes **2** and **3** should correspond to the observed ones, at about 463 nm. This mean that the observed bands about 462-478 nm don't correspond to same transition in the four complex, which is interpreted as hypochromic and hyperchromic effects of the substitution of methyl group by halogen atom. These substitutions have also hyperchromic effect on the observed bands at 422 nm for the complex **1**. The extinction of the band at 422 nm and observation of the other at 368 for complex **4** should be also interpreted as hypochromic and hyperchromic effects of the substitution of aromatic sulfonyl dithiocarbamate (*dtc*²⁻) by dithiolate derivatives (*ecda*²⁻). Unlike the experimental spectrum of complex **4** the calculated

band at 355 nm has feeble oscillator strength in the same range of the calculated bands with lower wave length. This discrepancy in relative intensities of bands between experimental and using CAM-B3LYP simulated was explained by Paes et al as probable defects in the model.³² The calculated bands at 332.5, 328.7, 332.6 and 333.9 nm are observed at 328, 324, 323 and 327 respectively for the complexes **1**, **2**, **3** and **4** respectively. Good agreement is noted between experimental and calculated intensities of these bands relatively to the others. For complexes **1**, **2**, and **3** these bands are mainly due to HOMO to LUMO transition. For the complex **4** the band is mainly due to transition from H-1 to LUMO. The compositions of these transitions orbitals help to explain why these d-d/MLCT/LLCT mixed characters bands are insensible to the modification of the R substituent. In simulated spectra only complex **4** absorbs at 316.9 and 308.2 nm. These bands are mainly ascribed to H-1→LUMO and HOMO→LUMO transitions. The strong contribution of cyanure and carboxylic groups to these orbitals explain why these bands don't appear in the simulated spectra of complexes **1**, **2**, and **3**. The bands calculated at 263.1 nm for complex **4** and 267.3 nm for complex **1** correspond to their observed one at 267 nm. These bands with mixed LMCT/ILCT/MLCT character correspond to transitions between orbitals located at dppf moiety and Ni and its first shell coordination atoms. From the calculation for complex **1** of lambda diagnostic parameter, which is 0.24, we can conclude that long-range charge transfer held in this transition.⁴⁸ Transitions with relatively large oscillator strength are calculated in the region of the not observed band at 267nm for complexes **2** and **3**.

The observable high energy bands with wave length low then 260 nm have intensities comparable to the observed at 267 nm when they are calculated with very low oscillator strength relatively to the calculated one about 267-263 nm. It is to note that in the calculation, in the high energy region where the density of transitions is large, many transitions present a lambda diagnostic parameter smaller than 0.30, indicating their long range charge transfer.⁴⁸

Conclusion

DFT and TDDFT modeling techniques have been used to investigate the geometry, frontier molecular orbitals and UV-Vis spectra of Ni(II) complexes. The influences of ligand substitution and solvent on electronic spectra have been assessed. The geometry optimization results are in good agreement with the experimental X-ray diffraction results. A distorted

planar square geometry of the first coordination shell of Ni ion is detected and the geometry parameters make these optimal structures favorable for π conjugation.

We show that for complexes **1-3**, the HOMOs are located on d orbitals of the Ni atom with some contributions of p orbitals from S atoms of the bidentate SCS ligand. The HOMO of complex **4** is a result of the same contributions additionally to π_{CN} and π_{CC} over **eye** ones. So, the HOMO orbital is more delocalized in complex **4** than in complexes **1-3** which can be interpreted as a result of the substitution of dte^{2-} by ecda^{2-} . The LUMOs have a mixed contribution of d_{xy} and $d_{x^2-y^2}$ of Ni atom, anti-bonding π^* orbital of the bidentate SCS part and π_{PC}^* and π_{CC}^* of *pph*. The calculations reveal that complexes **1-3** exhibit similar HOMO-LUMO gap, while complexes **4** shows a smaller one. From LUMO and HOMO energies we infer that the studied complexes would ensure efficient dye regeneration and exhibit sufficient driving force for electron injection in TiO_2 and I^-/I_3^- environment.

Simulated and experimental studied complexes spectra show significant agreement. As experimentally observed, computational results reveal that all complexes show several absorption bands in UV region and a very low absorption in the visible region. DFT and TD-DFT results help to explain the substituent effects on electronic spectra of the studied complexes. We have assigned the observed bands to their corresponding electronic transitions. It is pointed out that observed band at same wavelength of complexes **1** and **4** result from different transitions in the two complexes. Moreover, the calculated bands have been shifted upon the introduction of electron-donating substituent ecda^{2-} in complex **4** compared to the calculated spectra of complexes **1-3** containing dte^{2-} ligand.

Supplementary

Additional detailed data can be found in the supplementary materials: Choice of the functional for DFT calculations, solvent effect on the simulated spectra, Table of lambda diagnostic, optimized coordinates of the complexes.

Acknowledgements

A large part of quantum calculations were performed on the cluster of the Institut des Sciences Moléculaires de Marseille (*iSm2*) by Sefia BRAHIM during her stay in this laboratory. The authors acknowledge the University of Saida for supporting this stay by a student grant.

References

- (1) Sugathan, V.; John, E.; Sudhakar, K. *Renewable and Sustainable Energy Reviews* **2015**, *52*, 54. doi:10.1016/j.rser.2015.07.076
- (2) Graetzel, M.; Janssen, R. A.; Mitzi, D. B.; Sargent, E. H. *Nature* **2012**, *488* (7411), 304. doi:10.1038/nature11476
- (3) Basheer, B.; Mathew, D.; George, B. K.; Nair, C. R. *Solar Energy* **2014**, *108*, 479. doi:10.1016/j.solener.2014.08.002
- (4) Ahmad, M. S.; Pandey, A. K.; Rahim, N. A. *Renewable and Sustainable Energy Reviews* **2017**, *77*, 89. doi:10.1016/j.rser.2017.03.129.
- (5) Ye, M.; Wen, X.; Wang, M.; Iocozzia, J.; Zhang, N.; Lin, C.; Lin, Z. *Materials Today* **2015**, *18* (3), 155. doi:10.1016/j.mattod.2014.09.001
- (6) Freeman, G. R.; Williams, J. G. In *Organometallics and Related Molecules for Energy Conversion*; Springer, 2015; pp 29–59. doi:10.1007/978-3-662-46054-2_2.
- (7) Hara, K.; Koumura, N. *Alternative Energy Photovoltaics, Ionic Liquids, and MOFs* **2009**, 91.
- (8) Goswami, N.; Gogoi, P. K.; Bhattacharyya, M. K.; Saikia, D. *International Journal of Innovative Research and Development (ISSN 2278–0211)* **2012**, *1* (7), 92.
- (9) Chi, Y.; Wu, K.-L.; Wei, T.-C. *Chemistry – An Asian Journal* **2015**, *10* (5), 1098. doi:10.1002/asia.201403261.
- (10) Yamane, S.; Hiyoshi, Y.; Tanaka, S.; Ikenomoto, S.; Numata, T.; Takakura, K.; Haraguchi, T.; Palafox, M. A.; Hara, M.; Sugiyama, M. *J. Chem* **2017**, *11*, 135. doi:10.17265/1934-7375/2017.04.001.
- (11) Veronese, L.; Quartapelle Procopio, E.; Rossi, F. D.; M. Brown, T.; Mercandelli, P.; Mussini, P.; D'Alfonso, G.; Panigati, M. *New Journal of Chemistry* **2016**, *40* (3), 2910. doi:10.1039/C5NJ03000E.
- (12) Linfoot, C. L.; Richardson, P.; McCall, K. L.; Durrant, J. R.; Morandeira, A.; Robertson, N. *Solar Energy* **2011**, *85* (6), 1195. doi:10.1016/j.solener.2011.02.023.
- (13) Yella, A.; Lee, H.-W.; Tsao, H. N.; Yi, C.; Chandiran, A. K.; Nazeeruddin, M. K.; Diau, E. W.-G.; Yeh, C.-Y.; Zakeeruddin, S. M.; Grätzel, M. *Science* **2011**, *334* (6056), 629. doi:10.1126/science.1209688.
- (14) Kilinc, D.; Sahin, O.; Horoz, S. *Energy Sources, Part A: Recovery, Utilization, and Environmental Effects* **2018**, *1*. doi:10.1080/15567036.2018.1518357.
- (15) Nguyen, T.-D.; Lan, Y.-P.; Wu, C.-G. *Inorganic chemistry* **2018**, *57* (3), 1527. doi:10.1021/acs.inorgchem.7b02862.
- (16) de Souza, J. dos S.; de Andrade, L. O. M.; Müller, A. V.; Polo, A. S. In *Nanoenergy*; Springer, 2018; pp 69–106. doi:10.1007/978-3-319-62800-4_2.
- (17) Islam, A.; Sugihara, H.; Hara, K.; Singh, L. P.; Katoh, R.; Yanagida, M.; Takahashi, Y.; Murata, S.; Arakawa, H.; Fujihashi, G. *Inorganic chemistry* **2001**, *40* (21), 5371. doi:10.1021/ic010391y.
- (18) Soellner, J.; Čísařová, I.; Strassner, T. *Organometallics* **2018**. doi:10.1021/acs.organomet.8b00637.
- (19) Geary, E. A.; Yellowlees, L. J.; Jack, L. A.; Oswald, I. D.; Parsons, S.; Hirata, N.; Durrant, J. R.; Robertson, N. *Inorganic chemistry* **2005**, *44* (2), 242. doi:10.1021/ic048799t.
- (20) Singh, B.; Drew, M. G. B.; Kociok-Kohn, G.; Molloy, K. C.; Singh, N. *Dalton Trans.* **2010**, *40* (3), 623. doi:10.1039/C0DT00582G.
- (21) Yadav, R.; Waghadkar, Y.; Kociok-Köhn, G.; Kumar, A.; Rane, S. B.; Chauhan, R. *Optical Materials* **2016**, *C* (62), 176. doi:10.1016/j.optmat.2016.09.071.
- (22) Du, P.; Schneider, J.; Li, F.; Zhao, W.; Patel, U.; Castellano, F. N.; Eisenberg, R. *J. Am. Chem. Soc.* **2008**, *130* (15), 5056. doi:10.1021/ja711090w.
- (23) Singh, S. K.; Chauhan, R.; Diwan, K.; Drew, M. G.; Bahadur, L.; Singh, N. *Journal of Organometallic Chemistry* **2013**, *745*, 190. doi:10.1016/j.jorganchem.2013.07.072.
- (24) Sun, L.; Shu, S.; Zhou, Y.; Hou, S.; Liu, Y.; Ke, Z. *Materials* **2018**, *11* (11), 2192. doi:10.3390/ma11112192
- (25) Kumar, A.; Auvinen, S.; Trivedi, M.; Chauhan, R.; Alatalo, M. *Spectrochimica Acta Part A: Molecular and Biomolecular Spectroscopy* **2013**, *115*, 106. doi:10.1016/j.saa.2013.06.022.

- (26) Singh, V.; Chauhan, R.; Gupta, A. N.; Kumar, V.; Drew, M. G.; Bahadur, L.; Singh, N. *Dalton Transactions* **2014**, 43 (12), 4752. doi:10.1039/C3DT52142G.
- (27) A. Cameron, L.; W. Ziller, J.; F. Heyduk, A. *Chemical Science* **2016**, 7 (3), 1807. doi:10.1039/C5SC02703A.
- (28) Tsaturyan, A.; Machida, Y.; Akitsu, T.; Gozhikova, I.; Shcherbakov, I. *Journal of Molecular Structure* **2018**, 1162, 54. doi:10.1016/j.molstruc.2018.02.082.
- (29) Shen, W.-C.; Huo, P.; Huang, Y.-D.; Yin, J.-X.; Zhu, Q.-Y.; Dai, J. *RSC Advances* **2014**, 4 (104), 60221. doi:10.1039/C4RA10991K.
- (30) Gao, F.; Wang, Y.; Shi, D.; Zhang, J.; Wang, M.; Jing, X.; Humphry-Baker, R.; Wang, P.; Zakeeruddin, S. M.; Grätzel, M. *Journal of the American Chemical Society* **2008**, 130 (32), 10720. doi:10.1021/ja801942j.
- (31) Miao, Q.; Gao, J.; Wang, Z.; Yu, H.; Luo, Y.; Ma, T. *Inorganica Chimica Acta* **2011**, 376 (1), 619. doi:10.1016/j.ica.2011.07.046.
- (32) Paes, L. W. C.; Suárez, J. A.; Márquez, A. M.; Sanz, J. F. *Theoretical Chemistry Accounts* **2017**, 136 (6), 71. doi:10.1007/s00214-017-2098-7.
- (33) Sirbu, D.; Turta, C.; Benniston, A. C.; Abou-Chahine, F.; Lemmetyinen, H.; Tkachenko, N. V.; Wood, C.; Gibson, E. *RSC Advances* **2014**, 4 (43), 22733. doi:10.1039/C4RA03105A.
- (34) Chauhan, R.; Kociok-Köhn, G.; Trivedi, M.; Singh, S.; Kumar, A.; Amalanerkar, D. P. *J Solid State Electrochem* **2015**, 19 (3), 739. doi:10.1007/s10008-014-2660-3.
- (35) Wong, W. W. H.; Curiel, D.; Lai, S.-W.; Drew, M. G. B.; Beer, P. D. *Dalton Trans.* **2005**, 0 (4), 774. doi:10.1039/B416851H.
- (36) Kumar, A.; Chauhan, R.; Molloy, K. C.; Kociok-Kohn, G.; Bahadur, L.; Singh, N.; web-support@bath.ac.uk. *Chemistry - A European Journal* **2010**, 16, 4307. doi:10.1002/chem.200903367.
- (37) Schweinfurth, D.; Büttner, N.; Hohloch, S.; Deibel, N.; Klein, J.; Sarkar, B. *Organometallics* **2013**, 32 (20), 5834. doi:10.1021/om400429f.
- (38) Manar, K. K.; Gupta, A. N.; Gupta, A. K.; Prasad, L. B.; Srivastava, P.; Drew, M. G. B.; Singh, N. *ChemistrySelect* **2017**, 2 (9), 2655. doi:10.1002/slct.201700367.
- (39) Singh, A.; Singh, P.; Kociok-Köhn, G.; Trivedi, M.; Kumar, A.; Chauhan, R.; Rane, S. B.; Terashima, C.; Gosavi, S. W.; Fujishima, A. *New Journal of Chemistry* **2018**. doi: 10.1039/C8NJ00855H.
- (40) Becke, A. D. *The Journal of Chemical Physics* **1993**, 98 (7), 5648. doi:10.1063/1.464913
- (41) Jacquemin, D.; Preat, J.; Charlot, M.; Wathelet, V.; André, J.-M.; Perpète, E. A. *The Journal of chemical physics* **2004**, 121 (4), 1736. doi:10.1063/1.1764497.
- (42) Casida, M. E. In *Recent Advances in Density Functional Methods; Recent Advances in Computational Chemistry; WORLD SCIENTIFIC, 1995; Vol. Volume 1*, pp 155–192. doi:10.1021/jp0362335
- (43) Fantacci, S.; Migani, A.; Olivucci, M. *The Journal of Physical Chemistry A* **2004**, 108 (7), 1208.
- (44) De Angelis, F.; Fantacci, S.; Selloni, A. *Nanotechnology* **2008**, 19 (42), 424002. doi:10.1021/jp0362335
- (45) Adamo, C.; Jacquemin, D. *Chem. Soc. Rev.* **2013**, 42 (3), 845. doi:10.1039/C2CS35394
- (46) Jacquemin, D.; Perpète, E. A.; Scuseria, G. E.; Ciofini, I.; Adamo, C. *Journal of chemical theory and computation* **2008**, 4 (1), 123. doi:10.1021/ct700187z
- (47) Jacquemin, D.; Wathelet, V.; Perpète, E. A.; Adamo, C. *Journal of Chemical Theory and Computation* **2009**, 5 (9), 2420. doi.org/10.1021/ct900298e
- (48) Peach, M. J. G.; Benfield, P.; Helgaker, T.; Tozer, D. J. *The Journal of Chemical Physics* **2008**, 128 (4), 044118. doi:10.1063/1.2831900.
- (49) Yanai, T.; Tew, D. P.; Handy, N. C. *Chemical Physics Letters* **2004**, 393 (1–3), 51. doi:10.1016/j.cplett.2004.06.011.
- (50) Cossi, M.; Barone, V.; Cammi, R.; Tomasi, J. *Chemical Physics Letters* **1996**, 255 (4), 327. doi:10.1016/0009-2614(96)00349-1.
- (51) Frisch MJ, Schlegel GWTHB, Scuseria GE, Robb MA, Cheeseman JR, Scalmani G, Barone V, Mennucci B, Petersson GA, Nakatsuji H, Caricato M, Li X, Hratchian HP, Izmaylov AF, Bloino J, Zheng G, Sonnenberg JL, Hada M, Ehara M, Toyota K, Fukuda R, Hasegawa J, Ishida M, Nakajima T, Honda Y, Kitao O, Nakai H, Vreven T, Montgomery JA Jr, Peralta JE, Ogliaro F, Bearpark M, Heyd JJ, Brothers E, Kudin KN, Staroverov VN, Kobayashi R, Normand J, Raghavachari K, Rendell A, Burant JC, Iyengar SS, Tomasi J, Cossi M, Rega N, Millam JM, Klene M, Knox JE, Cross JB, Bakken V, Adamo C, Jaramillo J, Gomperts R, Stratmann RE, Yazyev O, Austin AJ, Cammi R, Pomelli C, Ochterski JW, Martin RL, Morokuma K, Zakrzewski VG, Voth GA, Salvador P, Dannenberg JJ, Dapprich S, Daniels AD, Foresman JB, Ortiz JV, Cioslowski J, Fox DJ (2009) Gaussian 09. Gaussian Inc., Wallingford.
- (52) Allouche, A.-R. *Journal of Computational Chemistry* **2011**, 32 (1), 174. doi: 10.1002/jcc.21600.
- (53) Pastorek, R.; Kameníček, J.; Pavlíček, M.; Husárek, J.; Šindelář, Z.; Žák, Z. *Journal of Coordination Chemistry* **2002**, 55 (11), 1301. doi:10.1080/0095897021000036406.

- (54) Oliveira, M. R. L.; De Bellis, V. M.; Fernandes, N. G. *Structural Chemistry* **1997**, *8* (3), 205. doi:10.1007/BF02263508.
- (55) Sathiyaraj, E.; Gurumoorthy, G.; Thirumaran, S. *New J. Chem.* **2015**, *39* (7), 5336. doi:10.1039/C4NJ02250E
- (56) Hoppenheit, R.; Lork, E.; Petersen, J.; Mews, R. *Chem. Commun.* **1997**, No. 17, 1659. doi:10.1039/A704174H.
- (57) Grätzel, M. *nature* **2001**, *414* (6861), 338.
- (58) Cahen, D.; Hodes, G.; Graetzel, M.; Guillemoles, J. F.; Riess, I. *The Journal of Physical Chemistry B* **2000**, *104* (9), 2053. doi: 10.1021/jp993187t
- (59) Sharma, R.; Yadav, B. S. 7. doi:10.9790/5736-08711117
- (60) F.1, S.-J. E.; 2; B.1, F. P. H.; 2; S.1, R. E. E.; R.1, C. N. M.; M.1, A. T.; 2; X, A.-J. J. *Journal of Chemical and Pharmaceutical Research* **2016**, *8* (7).
- (61) Kosar, B.; Albayrak, C. *Spectrochimica Acta Part A: Molecular and Biomolecular Spectroscopy* **2011**, *78* (1), 160. 10.1016/j.saa.2010.09.016.
- (62) Wu, J.; Song, Y.; Zhang, E.; Hou, H.; Fan, Y.; Zhu, Y. *Chemistry – A European Journal* **2006**, *12* (22), 5823. 10.1002/chem.200500905.
- (63) Reichardt, C. *Chemical Reviews* **1994**, *94* (8), 2319. doi:10.1021/cr00032a005

Draft

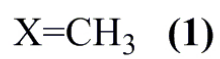
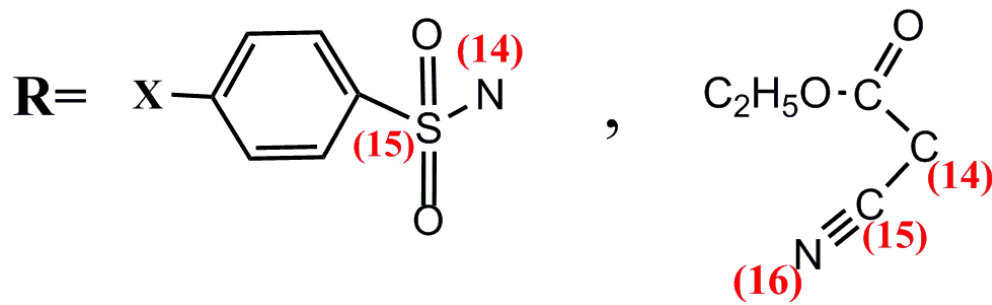
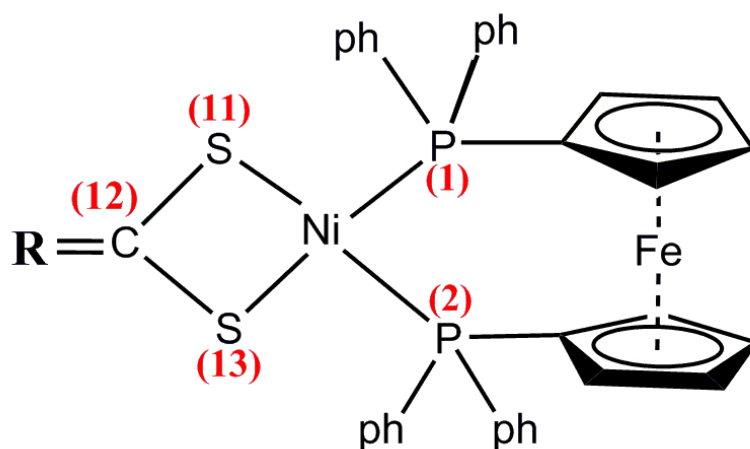
List of figures

- Figure 1: 2D structure of complexes **1-4** and nickel first coordination shell atoms numbering.
- Figure 2: Optimized structures of studied complexes (**1-4**).
- Figure 3: Main geometrical parameters obtained at the B3LYP/6-31G(d) level in CH₂Cl₂ on a model system
- Figure 4: The fourth Highest Occupied Molecular Orbital (HOMO) and Lowest Unoccupied Molecular (LUMO) of **1-4** complexes obtained with B3LYP.
- Figure 5: HOMO and LUMO energies obtained using B3LYP functional, TiO₂ conduction band energy⁵⁷ and the redox potential of I⁻/I₃⁻⁵⁸
- Figure 6: Decomposition analysis (in %) of the five highest occupied molecular orbitals of complexes **1-4** (B3LYP level). For each orbital, this decomposition expresses the main contributors of the complex (square: sulfur atoms belonging to the Ni first coordination shell, circle: Fe atom of the ferrocene, triangle up: Cps' of the ferrocene, triangle down: Nickel atom, diamond for the Cyanine). The color indicates the complex (1 in black, 2 red, 3 blue, 4 pink).
- Figure 7: Decomposition analysis (in %) of the five lowest unoccupied molecular orbitals of complexes **1-4** (B3LYP level). For each orbital, this decomposition expresses the main contributors of the complex (square: d's of the Nickel atom, circle: Sulfurs, triangles (up and down): Cps' of the ferrocene, diamond: the free Ph group, triangles (left and right) for parts specific to 4. The color indicates the complex (1 in black, 2 red, 3 blue, 4 pink).
- Figure 8: Superposition of experimental spectra of **1-4**, spectra produced via digitizing figures of reference²³ with authorization of its authors.
- Figure 9: Using CAM-B3LYP Calculated electronic absorption spectra (blue line) and digitized experimental electronic absorption spectra from ref²³ (red line) of complex **1**.
- Figure 10: Using CAM-B3LYP Calculated electronic absorption spectra (blue line) and digitized experimental electronic absorption spectra from ref²³ (red line) of complex **2**.
- Figure 11: Using CAM-B3LYP Calculated electronic absorption spectra (blue line) and digitized experimental electronic absorption spectra from ref²³ (red line) of complex **3**.
- Figure 12: Using CAM-B3LYP Calculated electronic absorption spectra (blue line) and digitized experimental electronic absorption spectra from ref²³(red line) of complex **4**.

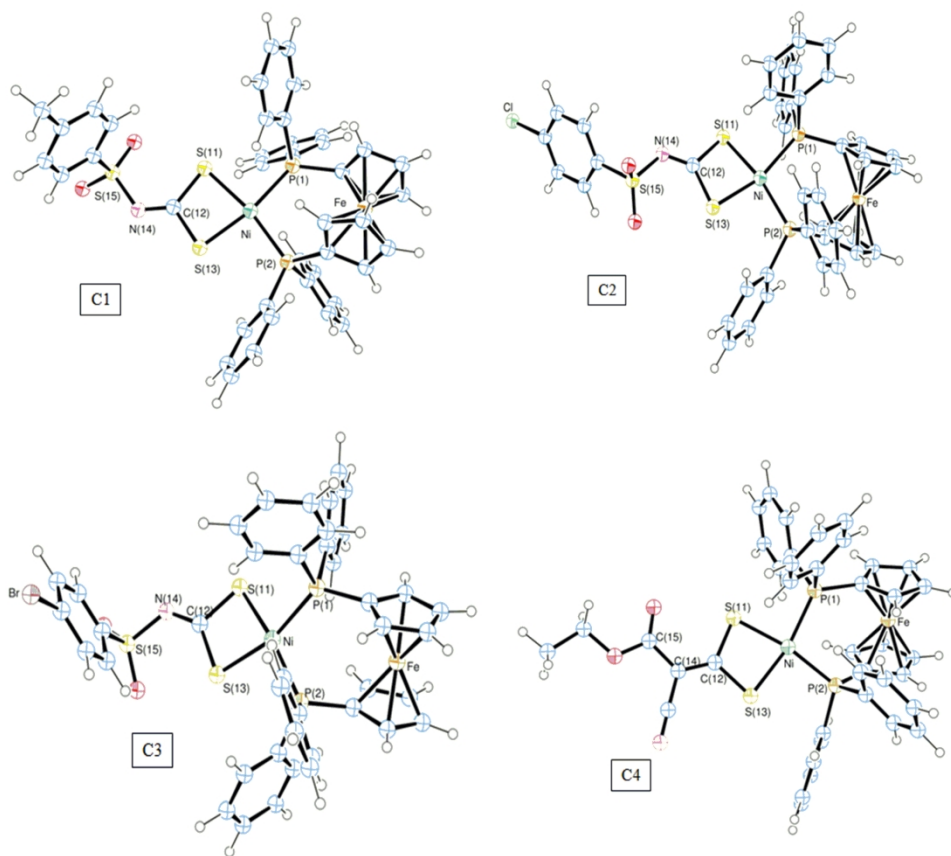
List of tables

- Table 1: Selected X-Ray²³ and optimized bond lengths (in Å) and bond angles (in °) of complexes **1-4**.

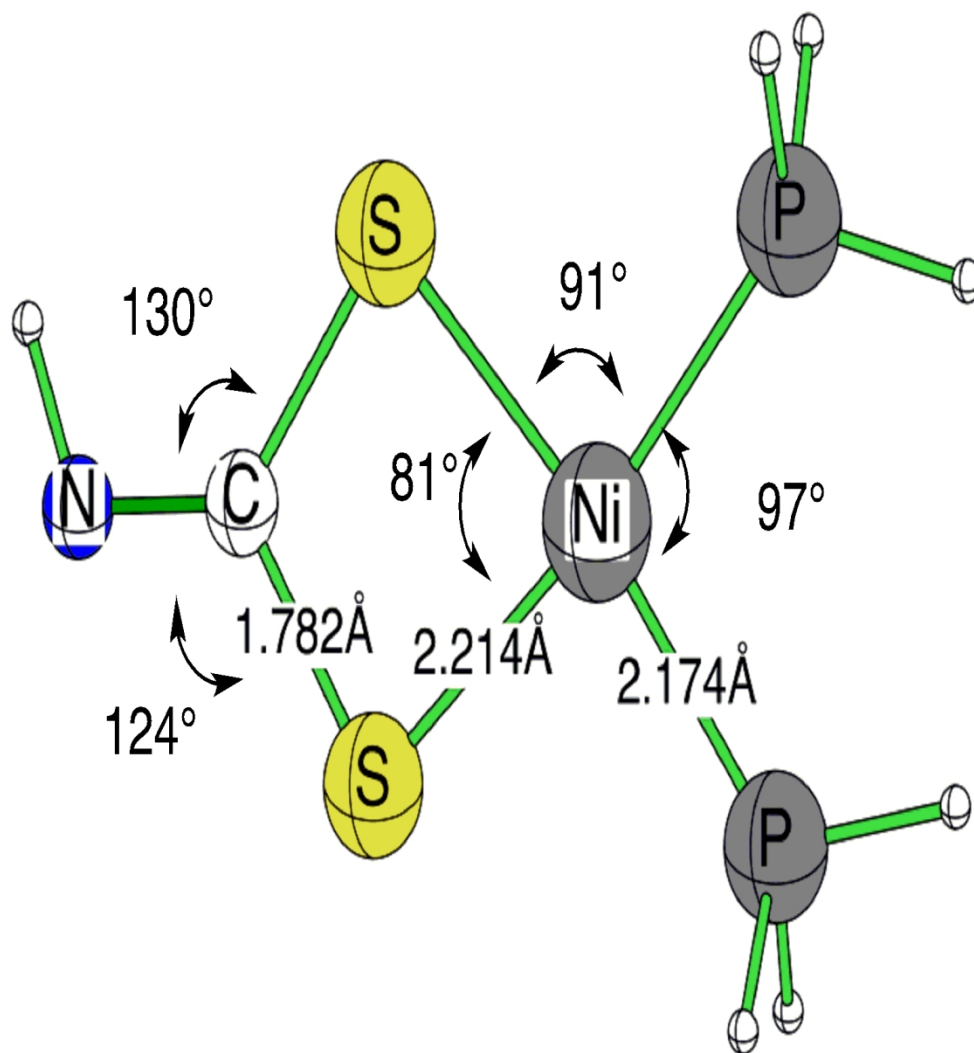
Draft



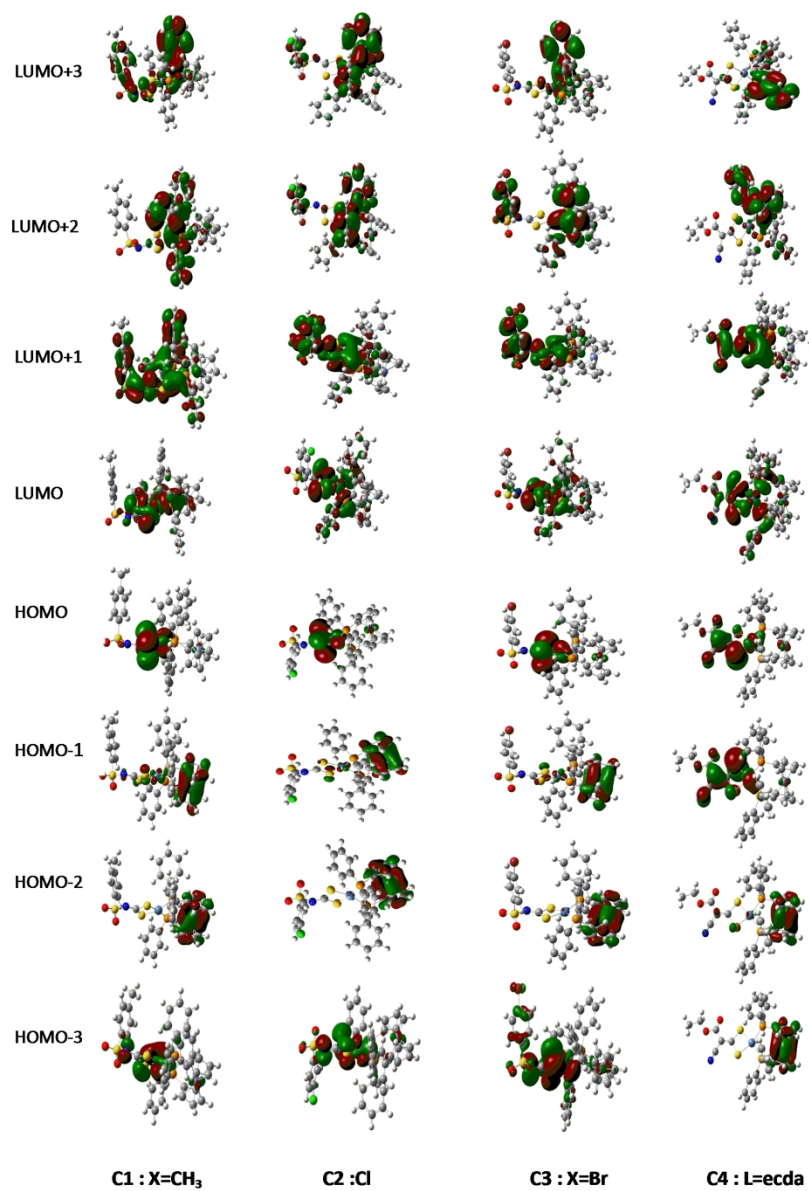
83x91mm (300 x 300 DPI)



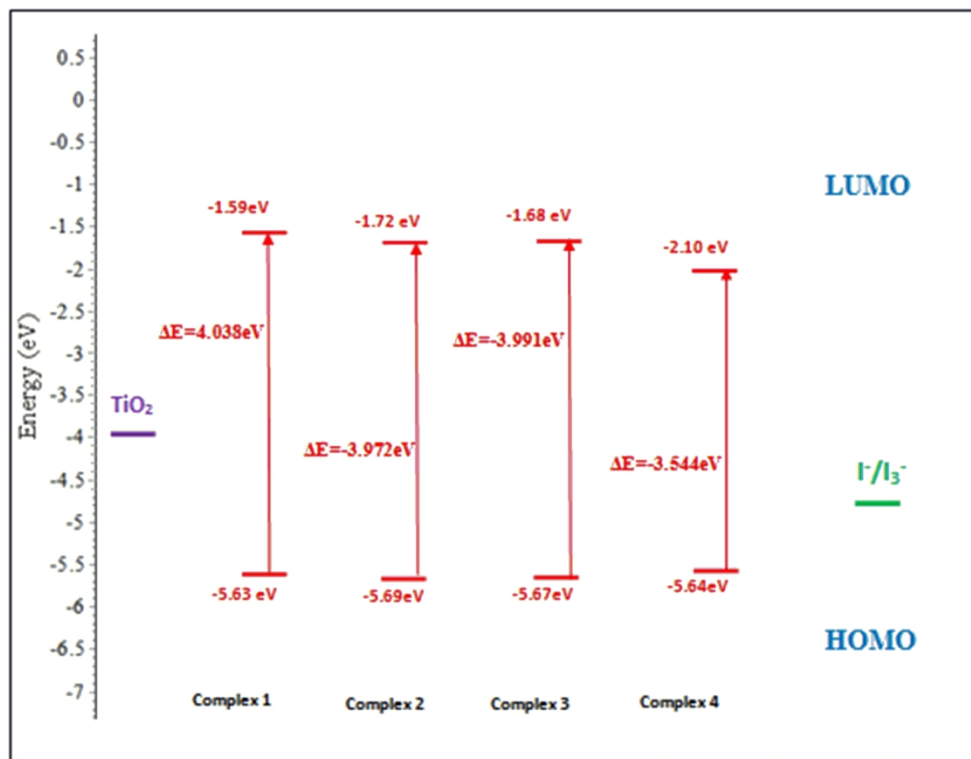
183x165mm (300 x 300 DPI)



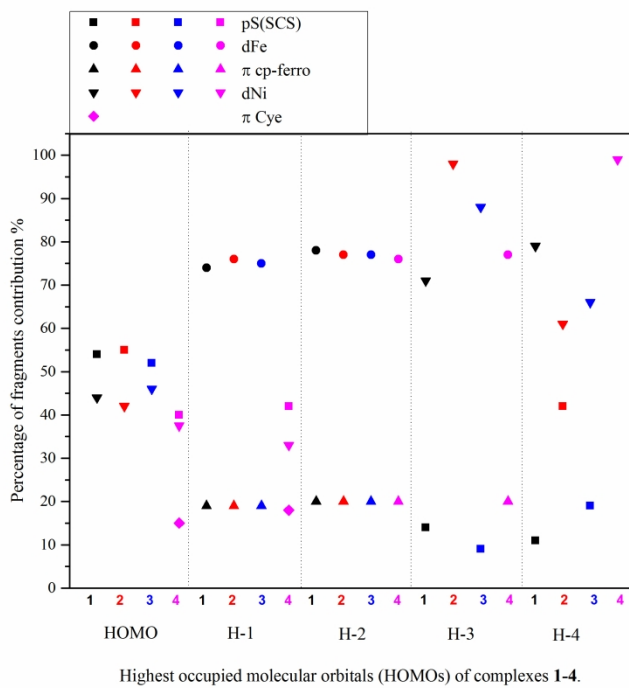
137x148mm (300 x 300 DPI)



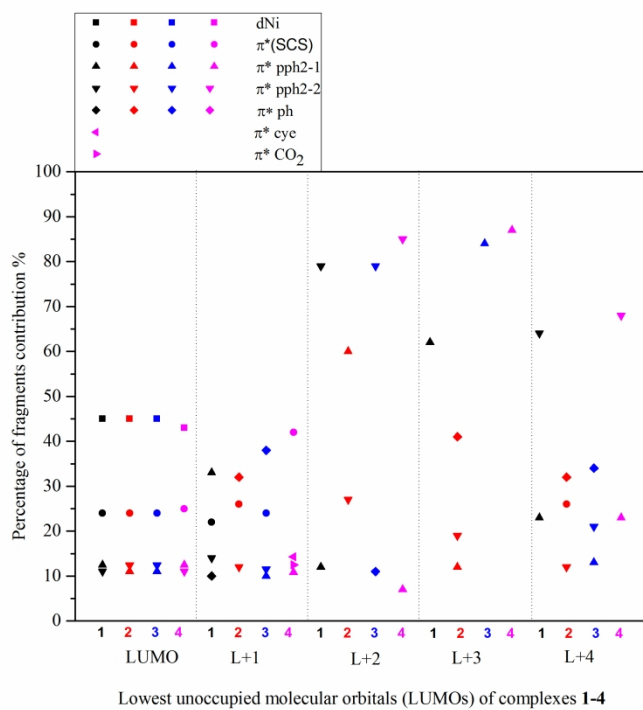
156x222mm (300 x 300 DPI)



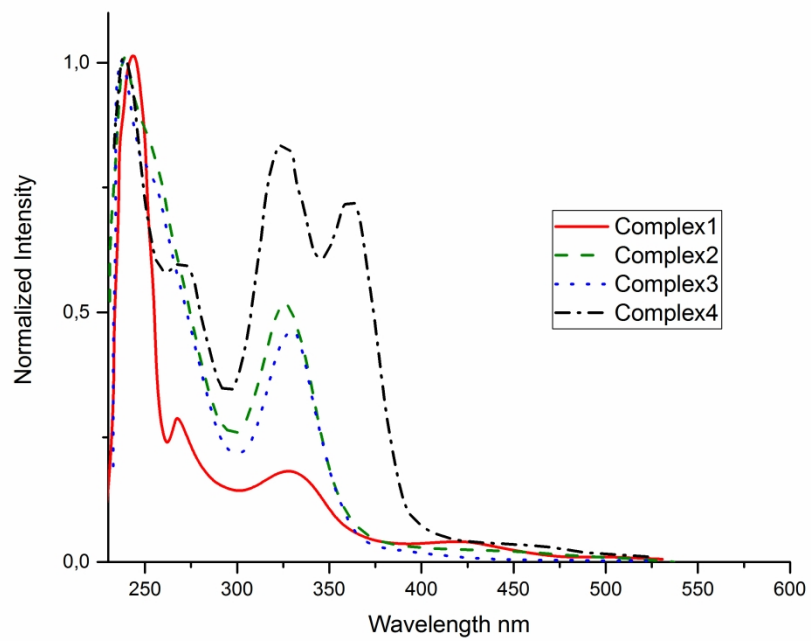
157x121mm (300 x 300 DPI)



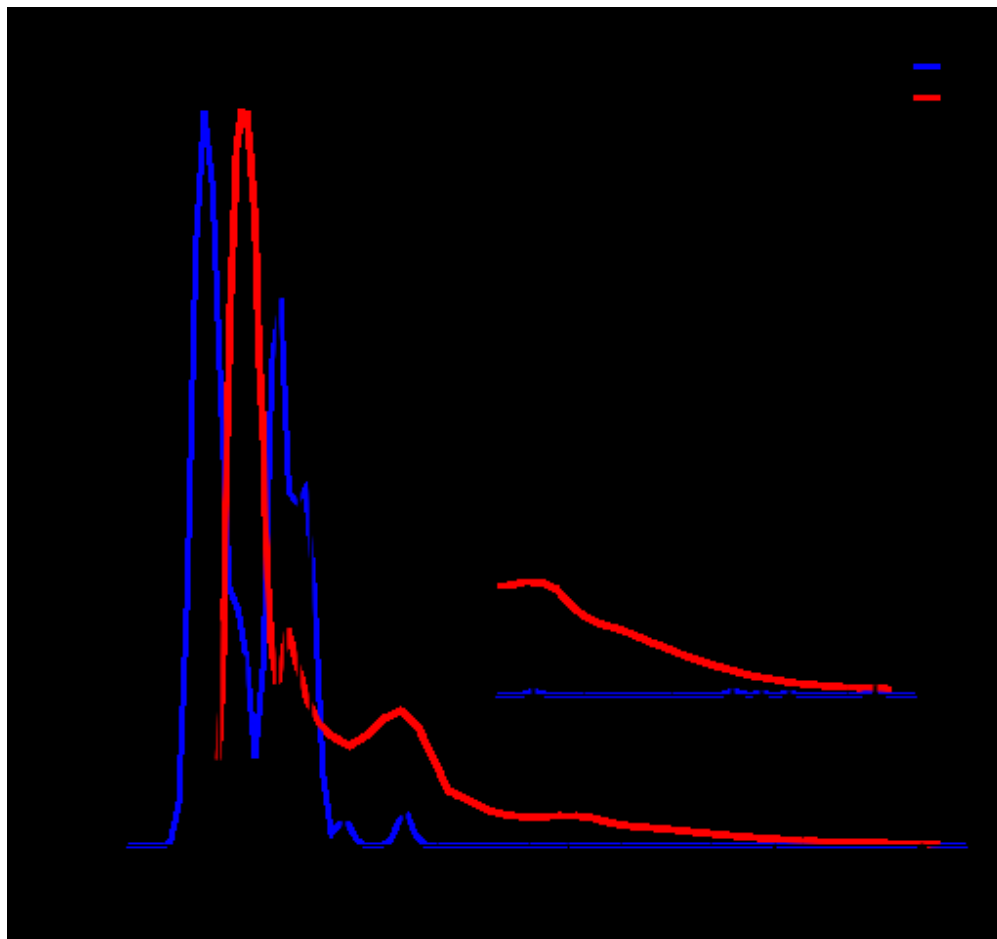
272x208mm (300 x 300 DPI)



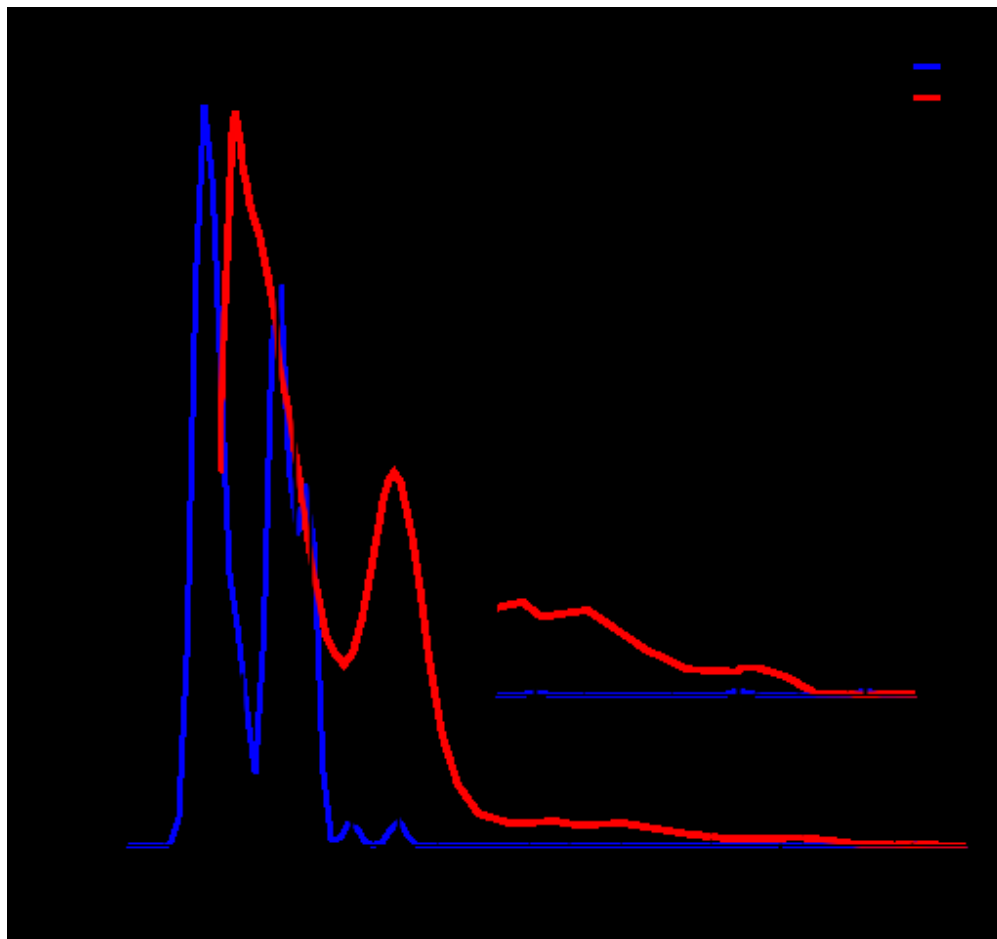
272x208mm (300 x 300 DPI)



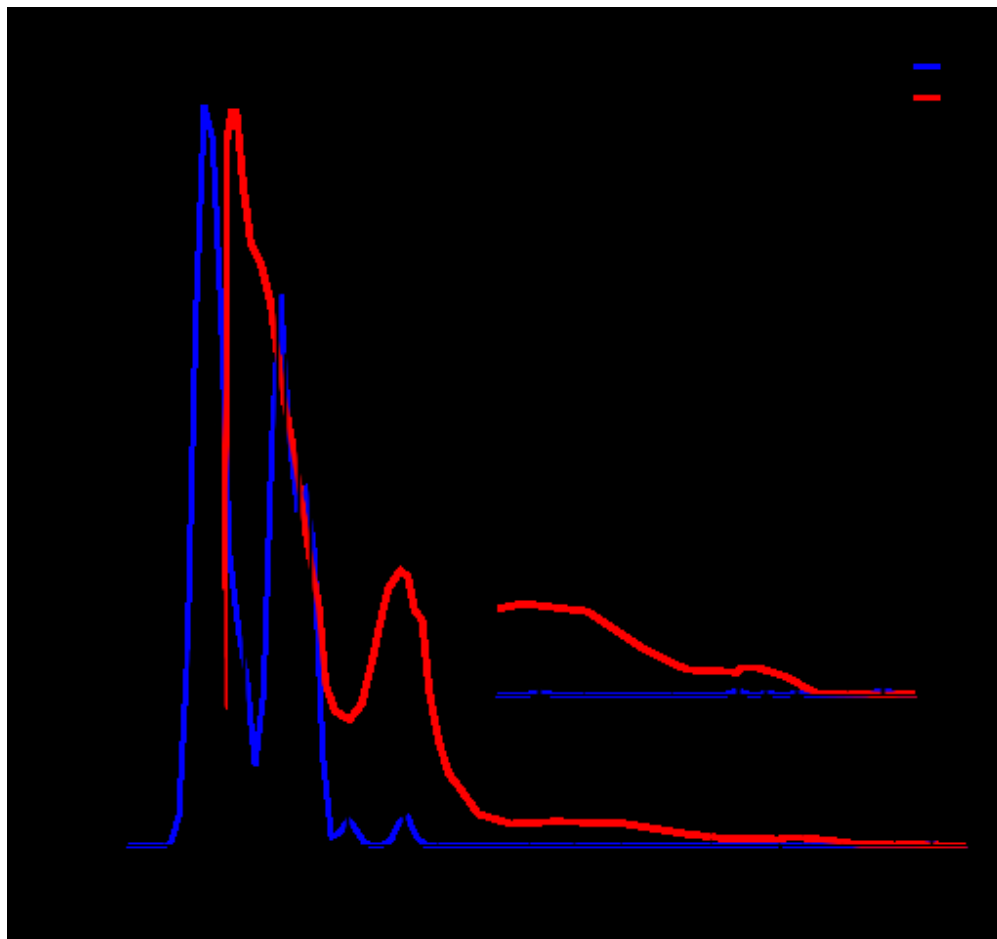
272x208mm (300 x 300 DPI)



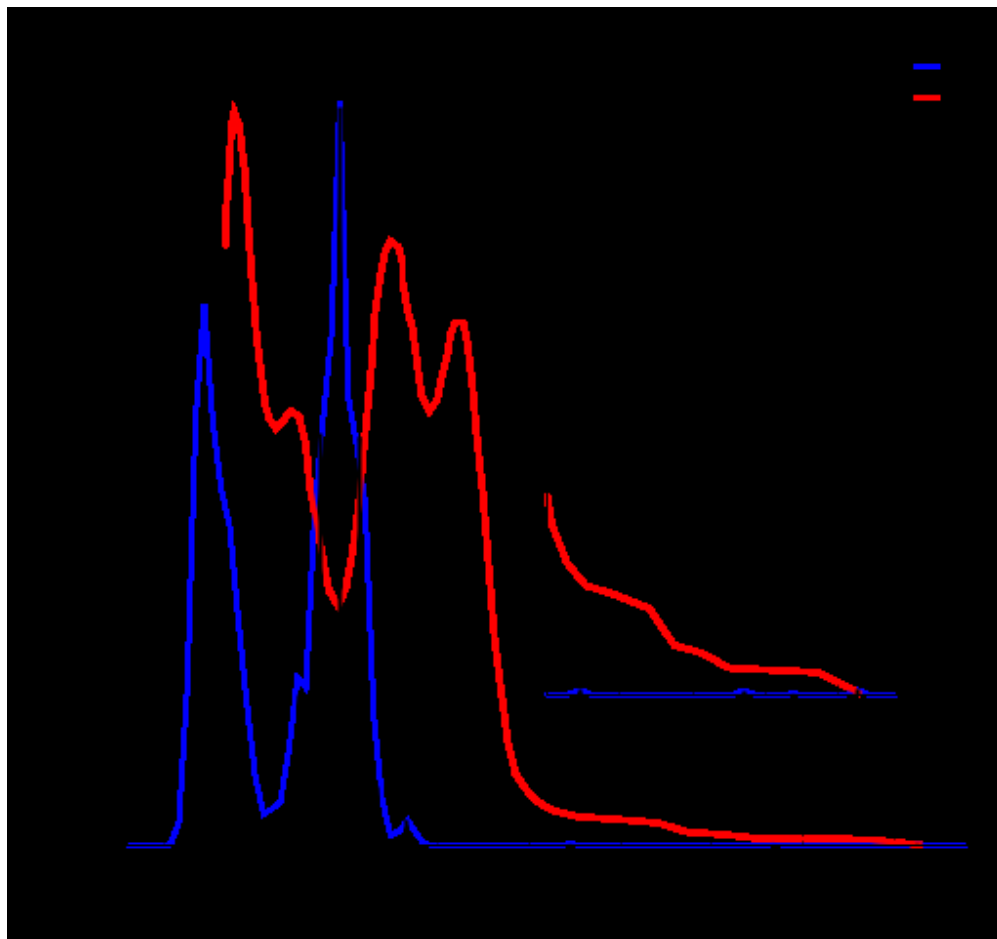
180x169mm (72 x 72 DPI)



180x169mm (72 x 72 DPI)



180x169mm (72 x 72 DPI)



180x169mm (72 x 72 DPI)

	Complex1		Complex2		Complex3		Complex4
	Gas	X-Ray	Gas	X-Ray	gas	X-Ray	Gas
	B3LYP		B3LYP		B3LYP		B3LYP
Bond lengths							
Ni-P(1)	2.224	2.216(1)	2.217	2.216(1)	2.219	2.223(1)	2.228
Ni-P(2)	2.216	2.207(1)	2.227	2.222(1)	2.228	2.231(1)	2.224
Ni-S(11)	2.229	2.211(1)	2.222	2.207(1)	2.221	2.207(1)	2.223
Ni-S(13)	2.218	2.201(1)	2.239	2.219(1)	2.230	2.211(1)	2.218
Bond angles							
P(1)-Ni-P(2)	102.06	101.85(6)	102.19	101.80(4)	101.78	101.75(3)	101.84
S(11)-Ni-P(1)	88.275	89.96(6)	91.53	93.15(4)	91.35	93.15(3)	91.92
S(13)-Ni-P(2)	91.72	90.61(6)	88.93	87.77(4)	89.99	87.96(3)	88.98
S(11)-Ni-S(13)	79.04	77.98(6)	78.84	77.85(4)	79.22	77.64(3)	78.39

Draft